JACS
JOURNAL OF THE AMERICAN CHEMICAL SOCIETY
pubs.acs.org/JACS
Article

Porous Dithiine-Linked Covalent Organic Framework as a Dynamic Platform for Covalent Polysulfide Anchoring in Lithium−Sulfur Battery Cathodes

Sattwick Haldar,* Mingchao Wang, Preeti Bhauriyal, Arpan Hazra, Arafat H. Khan, Volodymyr Bon, Mark A. Isaacs, Ankita De, Leonid Shupletsov, Tom Boenke, Julia Grothe, Thomas Heine, Eike Brunner, Xinliang Feng, Renhao Dong, Andreas Schneemann, and Stefan Kaskel*

Cite This: https://doi.org/10.1021/jacs.2c02346
Read Online
ACCESS | Metrics & More | Article Recommendations | Supporting Information

ABSTRACT: Dithiine linkage formation via a dynamic and self-correcting nucleophilic aromatic substitution reaction enables the de novo synthesis of a porous thianthrene-based two-dimensional covalent organic framework (COF). For the first time, this organo-sulfur moiety is integrated as a structural building block into a crystalline layered COF. The structure of the new material deviates from the typical planar interlayer π-stacking of the COF to form undulated layers caused by bending along the C−S−C bridge, without loss of aromaticity and crystallinity of the overall COF structure. Comprehensive experimental and theoretical investigations of the COF and a model compound, featuring the thianthrene moiety, suggest partial delocalization of sulfur lone pair electrons over the aromatic backbone of the COF decreasing the band gap and promoting redox activity. Postsynthetic sulfurization allows for direct covalent attachment of polysulfides to the carbon backbone of the framework to afford a molecular-designed cathode material for lithium−sulfur (Li−S) batteries with a minimized polysulfide shuttle. The fabricated coin cell delivers nearly 77% of the initial capacity even after 500 charge−discharge cycles at 500 mA/g current density. This novel sulfur linkage in COF chemistry is an ideal structural motif for designing model materials for studying advanced electrode materials for Li−S batteries on a molecular level.

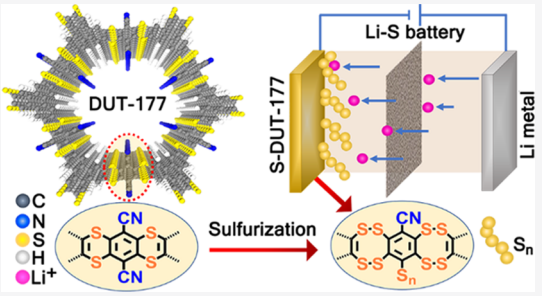

INTRODUCTION

Crystalline layered covalent organic frameworks (COFs) are porous materials consisting of highly symmetrical aromatic units linked within two dimensions (2Ds) by covalent bonds and are stacked into the third dimension (3D) by $\pi-\pi$ interactions.[1−7] Historically, starting from boroxines and boronate esters[8] and expanding to a multitude of different organic linkages including imines[9,10] and sp^2C-sp^2C connecting units,[11,12] the geometry and spatial arrangements of the building blocks of the 2D framework significantly depend on the orbital symmetry within these different linkages.[13] As a result, the overall COF skeleton and its structure-dependent properties are governed by their linkage chemistry. For instance, switching from C=C and C=N bonds to linkages based on fused aromatic rings enhances the structural rigidity of the COF layers and assists the electronic conjugation throughout the structure.[14,15] Additionally, the construction of 2D crystalline COFs from linkages consisting of aromatic heterocycles endows the resulting materials with interesting electronic and redox properties. Prominent examples of such aromatic heterocycles include dioxin,[16−18] phenazine,[19−21] oxazole,[22] thiazole,[23,24] benzimidazole,[25] or benzo-oxazole[26] linkages which affect the energy levels of the resulting material's band structure. This gives the opportunity to precisely engineer the band gap[25] of the framework via reticular chemistry for targeted use in applications such as photocatalysis,[27] electro-catalysis,[28] electronic devices,[29] and energy storage.[30−33]

In the case of sulfur-containing heterocycles, the vacant sulfur d-orbital can potentially interact with guest ions for charge storage, and the low electronegativity of sulfur also provides lone pair electrons for the C−S bond of the heterocycle. This can play an important role for the electronic conjugation, especially when it sustains in a radical cationic form.[34] Moreover, the moderate C−S bond strength facilitates chemical tunabilty via postsynthetic transformations. However, the poor stability of the S-rich frameworks and the instability of S-containing precursors hamper the engineering of crystalline frameworks via heterocycle ring-closing mechanisms. While

Received: March 2, 2022

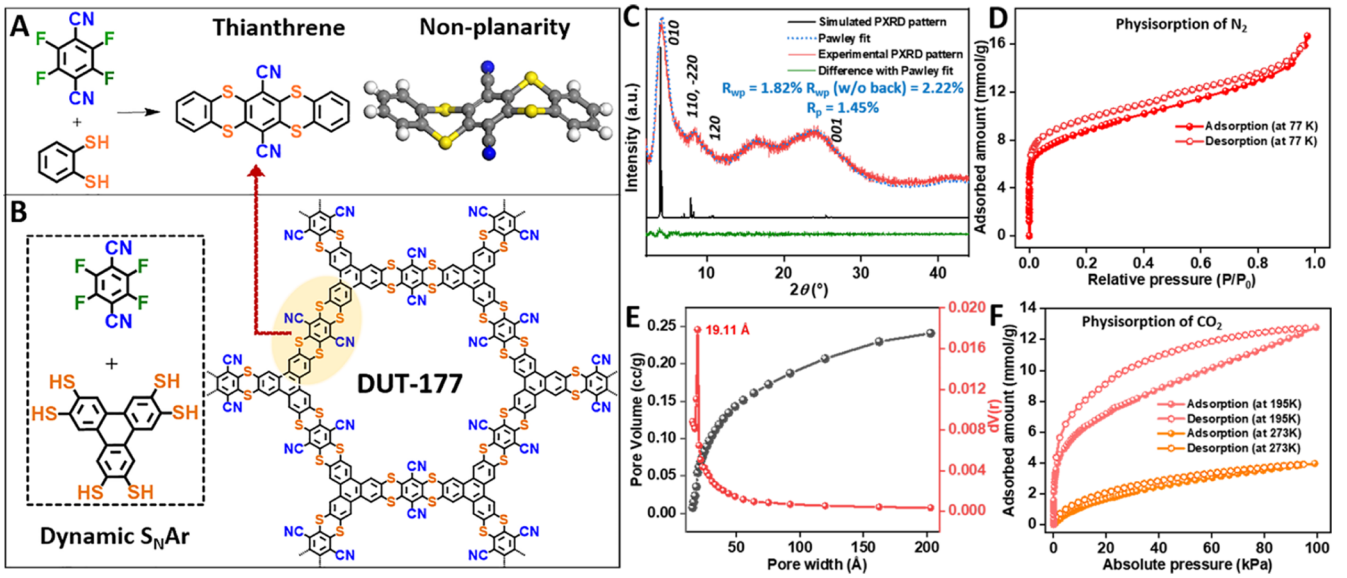

Figure 1. (A) Synthetic route toward the thianthrene model compound via an irreversible S_NAr reaction. C, H, N, and S are represented in gray, white, blue, and yellow, respectively. (B) Synthetic route toward the thianthrene-based COF named DUT-177. (C) Comparison of the experimental PXRD pattern (red) of DUT-177 with the simulated pattern (black). The experimental pattern was fit via the Pawley method (blue, fit; green, difference). (D) N_2 physisorption isotherm N_2 of DUT-177 recorded at 77 K. (E) Pore width and cumulative pore volume distribution obtained through the BJH method from the desorption branch of the N_2 isotherm at 77 K. (F) Physisorption of carbon dioxide (CO_2) on DUT-177 at 195 and 273 K. Filled and empty symbols in physisorption isotherms represent ad- and desorption branches. Lines connecting the measurement points are a guide for the eye and do not have any physical meaning.

oxazole-, thiazole-, and benzo-oxazole-containing 2D COFs follow similar ring closures, they are constructed mainly from *ortho*-hydroxy-/thiol-substituted arylamines.[22,26,35] However, free rotation along the single bond there disrupts the electronic conjugation in the layer. In contrast to this, the phenazine linkages formed by reacting diketones with ortho-diamines yield aromatic and planar frameworks, but long-range periodic order is hindered due to the relatively low crystallinity caused by low reversibility during cyclization.[19] However, some advances have been recently made using dynamic covalent chemistry.[36]

COF formation by ring cyclizations offers additional stability due to the connecting fused aromatic rings which allow the framework to withstand the harsh conditions of postsynthetic modification.[37,38] Also, fused heterocycles containing p block elements (O, S, Se, or P) would propel COFs toward applications exploiting their electronic properties.[39−41] The design of suitable linkers and the optimization of reaction conditions for COF construction remains a demanding task for synthetic chemists. The dioxin linkage formation in a 2D COF by irreversible nucleophilic aromatic substitution (S_NAr) between diol- and difluoro-functionalized linker molecules was established by Yaghi and co-workers in the synthesis of COF-316.[18] This is a prime example of a fused heterocyclic organic linkage building up crystalline and very stable COFs. This linkage has been suggested for various applications ranging from catalysis to energy storage devices.[17,18,42,43] The transfer of this irreversible ring-closing mechanism for developing crystalline COFs with other heterocyclic linkages remains an open challenge.

In this work, a novel dithiine-linked 2D thianthrene COF (DUT-177) is constructed by S_NAr of an aromatic *ortho*-aryldifluoride with *ortho*-aryldithiol nucleophiles showing strikingly different chemical and electronic properties compared to analogous COF-316. Although dithiine linkages have been constructed following the dynamic and self-correcting covalent chemistry reported by Swager and Ong, the crystalline nature of DUT-177 conveys more insights into the structure and properties.[44] The thianthrene structure is known to show a reversible conversion from a nonplanar to a planar state upon oxidation.[45] Hence, DUT-177 obtained from this thianthrene unit also shows anomalous nonplanar undulated layers in its neutral form which is exceptional, featuring unique weak nonplanar aromaticity. The sulfur skeleton of the thianthrene-based COF, its reversible redox properties, unique electronic features, and the presence of polar functionality (nitrile) are well suited for charge storage applications.[46] The systematic investigation of the possible chemical conversion of thianthrene to dithianthrene structures upon sulfurization is described to facilitate reversible lithiation chemistry in lithium−sulfur (Li−S) batteries. Detailed experimental studies assist in understanding this conversion precisely. In addition to the linkage conversion, further sulfur is attached to the COF backbone in the form of polysulfide chains. The covalent anchoring minimizes the polysulfide shuttle under charge−discharge conditions. The high-sulfur-content framework serves as a sulfur cathode in a Li−S battery with a deliverable specific capacity of 700 mA h/g_{sulfur} at 100 mA/g_{sulfur}. Furthermore, the material retains 76% of the specific capacity over 500 continuous charging−discharging cycles, highlighting the potential of thianthrene-based COFs for charge storage applications.

RESULTS AND DISCUSSION

Synthesis and Characterization. Inspired by the synthesis established by Yaghi and co-workers[18] for COF-316 by reacting a 3-connecting hexahydroxy linker (2,3,6,7,10,11-hexahydroxytriphenylene) with a 2-connecting aryl-tetrafluoride (2,3,5,6-tetrafluoroterephthalonitrile), we prepared a COF with a dithiine linkage (known as thianthrene). For the

https://doi.org/10.1021/jacs.2c02346
J. Am. Chem. Soc. XXXX, XXX, XXX−XXX

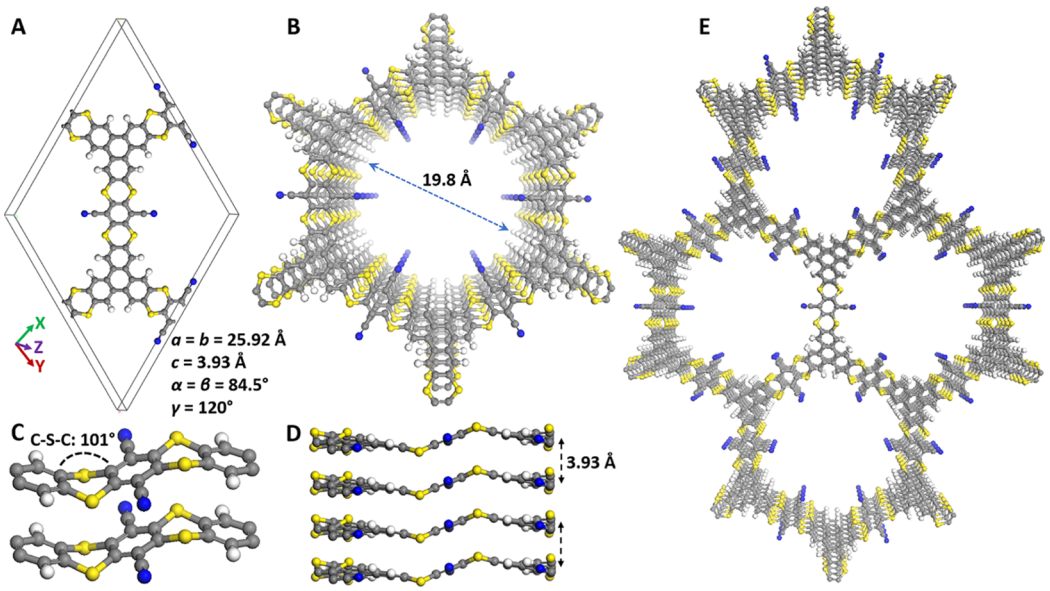

Figure 2. (A) Geometry and energy-minimized unit cell of DUT-177. (B) A portion of DUT-177 shows its 1D porous nanochannel. (C) Visualization of the buckling of the layers of DUT-177 along the dithiine linkage. The repulsion of the lone pairs of sulfur increases the intralayer distance. (D) The columnar view of DUT-177 along the *c*-axis shows the wavy stacking. (E) The 3D view of the 2D layered structure of DUT-177 shows uniform distribution of honeycomb-type pores. C, H, N, and S are represented in gray, white, blue, and yellow, respectively.

synthesis of the thianthrene-based COF, 2,3,6,7,10,11-triphenylenehexathiol, previously used for the construction of 2D MOFs,[47−49] was combined with 2,3,5,6-tetrafluoroterephthalonitrile in a sealed ampoule at elevated temperatures (see the Supporting Information for details). The obtained orange powder was termed DUT-177 (DUT—Dresden University of Technology). In parallel, the dynamic and self-correcting S_NAr reaction between *ortho*-aryldithiols (benzene-1,2-dithiol) and *ortho*-aryltetrafluorides (2,3,5,6-tetrafluoroterephthalonitrile) was used to prepare a novel model compound which also contains the dithiine linkage (Figure 1A and Scheme S1). Unlike the dioxin-linking structures reported, the C−S−C units in dithiine are stabilized in a nonplanar configuration to minimize sulfur's lone pair electron repulsion (Figure S1).[17,18] Single crystals grown from the model compound (a novel molecule) allowed us to verify this nonplanar configuration (Figures 1A and S1, for crystal structure data, see Table S1, CCDC-2149889). The structural model of DUT-177 was simulated in silico and experimentally verified by powder X-ray diffraction (PXRD) patterns (Figures 1C and 2), confirming the formation of a periodic honeycomb structure analogous to the known dioxin-linked COF-316 with thianthrene repeating units in its skeleton (Figures 1B and S2 and Scheme S2).

The chemical integrity of this dithiine linkage and the cyano substitution in DUT-177 are evidenced by comparison with the model compound based on infrared spectroscopy (IR), Raman spectroscopy, and cross-polarization magic angle spinning carbon-13 nuclear magnetic resonance (CP-MAS-^{13}C NMR) (Figures S3 and S4). The powdered sample was washed thoroughly, purified, and activated by solvent exchange and supercritical drying for the spectrochemical studies (Section 2 of the Supporting Information). The characteristic signals of the carbon−sulfur linkage appeared at 694 and 717 cm^{-1} in the IR and Raman spectra, respectively, and at 141 ppm in ^{13}C NMR for the thianthrene-based COF, and a slight shift of the signal position was noticed for the model dithiine-linked compound. The nitrile functionality of DUT-177 and the model compound appeared in the IR spectrum at 2227 cm^{-1}, and the ^{13}C NMR featured a doublet signal at 114 ppm. Numerous asymmetric stretching bands of the carbon−sulfur bond and the nitrile functionality in the Raman spectra indicate different vibrational splittings of the energy states of the C−S bond associated with the bending or out-of-plane twisting of the bonds. PXRD measurements reveal reasonable crystallinity of the thianthrene-based COF DUT-177, even though the used S_NAr reaction is not as reversible as many of the literature known polycondensation reactions for imine, imide, oxazole, or benzimidazole linkage formation (Figure 1C and Scheme S2). The highly intense reflection at 2θ = 4.01° and the respectively lower intensity reflections observed at 2θ = 8.2, 16.39, and 24.3° verify the formation of a crystalline COF analogous to the honeycomb structure of the dioxin-linked material COF-316. The shifting of the reflection signifying the π-stacking distance at lower 2θ (24.3°) in comparison to that in the simulated pattern suggests the weakening of the interlayer interaction and increased probability of layer slipping. The simulated pattern and the fit of the experimental PXRD pattern via the Pawley method[50] with starting values obtained from the modeled structure illustrate a slight deviation of the experimental structure of DUT-177 from its ideal conformation caused by the reduced stacking interactions of the thianthrene unit compared to those of a fused aromatic ring (Figures S5−S13). Despite the slipping possibility of the layers, DUT-177 still generates nanoporous one-dimensional (1D) channels across the plane with a Brunauer−Emmett−Teller (BET) surface area of 709 $m^2\ g^{-1}$ calculated from N_2 physisorption at 77 K (Figures 1D and S14). This surface area is slightly higher than that reported for COF-316 which amounts to 557 $m^2\ g^{-1}$. The nanochannels have a pore width of ∼19 Å, which was estimated by the Barrett−Joyner−Halenda (BJH) method using the desorption branch of the isotherm (Figure 1E). The hysteresis in the N_2 (77 K) and CO_2 (195 K) isotherms indicates welling effects typical for porous polymers (Figure 1F). Elevation of the

https://doi.org/10.1021/jacs.2c02346
J. Am. Chem. Soc. XXXX, XXX, XXX−XXX

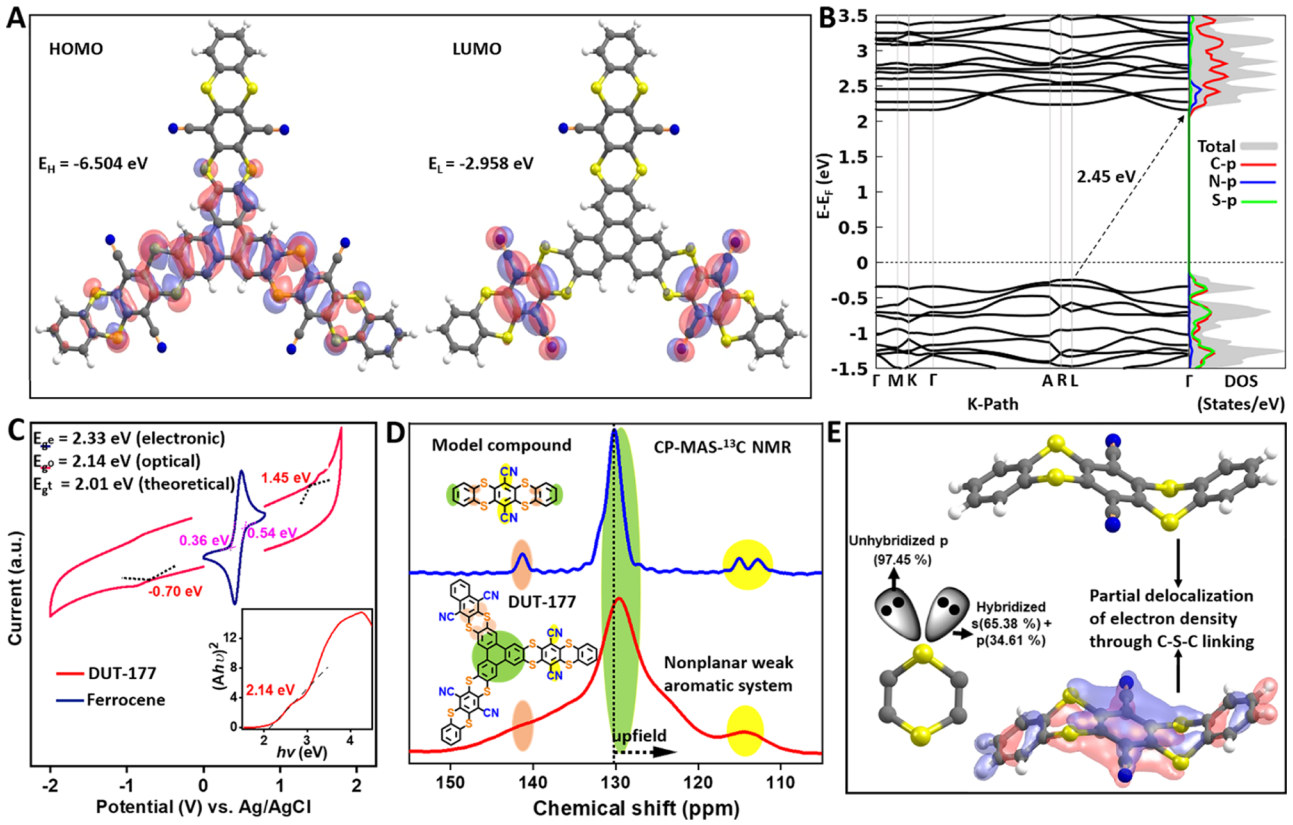

Figure 3. (A) Distribution of the HOMO and LUMO on the molecular unit of DUT-177 and the corresponding energies. (B) Electronic band structure analysis of AA-inclined stacked DUT-177 calculated using the HSE06 functional. (C) The oxidation−reduction potential from nonaqueous CV measurements of DUT-177 denotes the energies of the HOMO and LUMO and the electronic band gap. (Inset) The Tauc plot obtained from the UV−vis absorption spectra of DUT-177 used to determine the optical band gap. (D) CP-MAS-^{13}C NMR of the aromatic region of DUT-177 and its model compound (full range in the Supporting Information). (E) Theoretically calculated hybridization of available lone pairs of sulfur in dithiine linkage.

measurement temperature to 273 K significantly reduced the hysteresis, leading to a reversible adsorption−desorption profile of CO_2.

Structure Analysis. The crystallinity and repeating order of DUT-177 can be modeled in the preferred symmetrical unit cell, and a comprehensive analysis of the structure−property relationship was conducted via geometry and energy optimization. The dithiine linkage in 2D COFs is still unexplored, and unique structural properties compared to other highly π-stacked COFs are expected. The molecular structure of the dithiine-linked model compound, derived from single-crystal X-ray diffraction data, shows that the dithiine bridge induces nonplanarity in the structure (Figures 1A,B and S1). The out-of-plane bending of these two S−C bonds has a 101° dihedral angle (Figure 1C). The theoretically studied molecular unit of DUT-177 verifies the out-of-plane bending with the possibility of forming two energetically indistinct isomers depending on the thianthrene arrangements (up-down bending and all-up-all-down bending of the thianthrene ring; studied using Gaussian[51]). These two isomers can reversibly interchange by overcoming the low energy barrier of 5.06 kcal mol^{-1} (Figure S5 and Supporting Information VII). These two isomeric units periodically repeat to form two different arrangements of monolayers of DUT-177, defined as monolayer-1 and monolayer-2 in Figures S6 and S7, which are also indistinguishable in energetic stability (Table S3). However, once the single layers are π-stacked to form the layered thianthrene COF, only the structural arrangement from monolayer-1 retains its stability (see Supporting Information VII and Figure S8). Therefore, monolayer-1 was used to simulate the possible stacking orders of DUT-177 which are AA-eclipsed, AA-inclined, AA-serrated, and AB-staggered conformers (Figure S8 and Table S4). Though the symmetrical stacking of the layers builds the periodic structure in the $C2/m$ space group, the density functional theory results show that the AA-inclined stacking geometry is energetically favored in the $P1$ space group (Figure 2 and Tables S4 and S5), and its calculated PXRD pattern (Figures 1C, S9, and S10) agrees well with the experimental PXRD. The corresponding unit cell parameters are $a = b = 25.92$ Å, $c = 3.93$ Å, $\alpha = \beta = 84.9°$, and $\gamma = 120°$, indicating long-range ordering along the ab-plane. Interestingly, in this lowest energy structure, the layer flexes around the carbon−sulfur bond in the thianthrene unit and shows bending in two different directions to form a wavy 2D stacking (Figure 1B). The thianthrene and triphenylene units from adjacent layers are π-stacked at a distance of 3.95 Å (excluding van der Waals radii of atoms), which retains identical layer distances throughout the structure and generates a 1D nanochannel (Figure 1C,D). The 2D layers of the sheets of the powdered DUT-177 agglomerate or stack onto each other to different extents, leading to the irregular shape and patterns of the crystallites which were observed from the field emission scanning electron microscopy images (Figure S11). The columnar π-stacking of the eclipsed structure along the c-axis supports the small offset between the simulated and experimental PXRD results due to

https://doi.org/10.1021/jacs.2c02346
J. Am. Chem. Soc. XXXX, XXX, XXX−XXX

higher slipping of the layers (Figure S10). This is also supported by the lattice fringes detected by transmission electron microscopy (TEM) on the surface of the crystallites which are not much prominent due to the lower extent of ordered stacking (Figures S12 and S13). Since the wavy stacking is not expected to be strong enough to keep the layers at precise distances in the solvent-free activated sample, it is hypothesized to increase in comparison to the ideal structure, and the diffraction peaks representative of the layer stacking along the *c*-axis (between 2θ = 20 and 30°) shift to lower angles in the experimental PXRD pattern. However, the 3D propagation of the 2D structure originates from the numerous micropores with a lot of polar functional groups (sulfur- and cyano-containing rings) immobilized at the pore walls of DUT-177 (Figure 2E). The pore dimension (~19 Å) estimated from the N_2 physisorption at 77 K also matches well with the Connolly surface of the proposed structure taking the van der Waals radii of the atoms into account.

The dithiine linkage impacts the electronic energy levels of the COF and triggers redox activity at its sulfur center. The redox activity and electron transfer mechanism of the COF mostly depend on the electron density distribution of the orbitals of the building units. A closer look at the orbital energy diagram of the molecular units of DUT-177 (calculated using Gaussian) shows that the highest occupied molecular orbital (HOMO) is delocalized over the π-conjugated backbone, whereas the lowest unoccupied molecular orbital (LUMO) is localized on the nitrile-substituted benzene ring (Figures 3A and S15). Also, the electronic band structure analysis of DUT-177 monolayers (monolayer-1 in Figure S16) shows small dispersion in the valence band (VB) along with a dispersionless conduction band (CB), indicating a comparatively smaller in-plane effective mass of holes and large effective mass for electrons. The localization of the LUMO mainly causes this flat CB in DUT-177's monolayer-1. However, the situation changes when this monolayer-1 is stacked in an AA-inclined fashion in DUT-177, where an appreciable dispersion of the band structure due to the interlayer $\pi-\pi$ interaction (Figure 3B) is observed. The band gap of DUT-177 [calculated by the Perdew–Bruke–Ernzerhof (PBE) functional][52] is narrowed down to 1.62 eV (Figure S16C) with respect to monolayer-1 (2.01 eV) (Figure S16A). However, the actual band gap of 2.40 eV was obtained by the inclusion of the HSE06 functional results (Figure 3B),[53] which is in close accordance with the experimentally obtained value of 2.33 eV using cyclic voltammetry (CV) measurements (Figure 3C). Here, the calculated band structure reveals anisotropic transport in the stacked geometry, with a small in-plane and finite out-of-plane charge transport. The onset oxidation and reduction potentials of the COF can be related to the electronic energy level of the COF. The CV measurement was carried out under an inert atmosphere using a nonaqueous electrolyte system which indicates the position of the HOMO and LUMO energy levels (3.56 and 5.89 eV, respectively) and the corresponding band gap (2.33 eV) of the COF powder (Figure 3C). A Tauc plot considering the maximum wavelength of the UV–vis absorption of the COF shows the position of the band edge at 2.16 eV, which is also comparable to the theoretical band gap (Figure 3C, inset, and Figures S16 and S17). On the other hand, the strong delocalization of the electron density along the sulfur bridge interconnects the aromatic ring current throughout the 2D layer of DUT-177. This results in a significant line broadening and poor resolution of the ^{13}C NMR signals of the COF compared to those of the model compound at 300 and 800 MHz (Figure 3D), respectively. This broadening of the characteristic ^{13}C NMR signal of the thianthrene-based COF is also attributed to the strong anisotropy of the bulk magnetic susceptibility of the layered COF material. COF materials having a layer-type structure can exhibit a strong anisotropy of the bulk magnetic susceptibility.[54,55] For this reason, further line narrowing of the COF sample is not possible. The line narrowing factor, υ, can be written as $\upsilon = \Delta\upsilon_{1/2}^{MAS}/\Delta\upsilon_{1/2}^{Static} = 1/3|\Delta\chi/\overline{\chi}|$, where $\Delta\chi = |\chi_{\perp} - \chi_{\parallel}|$ denotes the anisotropy and $\overline{\chi} = 1/3(2\chi_{\parallel} + \chi_{\perp})$ is the isotropic average of the bulk magnetic susceptibility.[56]

The impact of the extended conjugation is not prominent in the case of the model system since the aromatic ring current is terminated. Consequently, the NMR signals of the model compound appear at the expected positions and are well resolved. This similarity in the signal pattern of the model compound with the deconvoluted signals of the COF helps to identify the presence of the cyano functional group and the carbon–sulfur bridges in the CP-MAS-^{13}C NMR of DUT-177. The presence of the aromatic ring current is expected to contribute to the push–pull electronics between the thianthrene moiety and the nitrile substituents on DUT-177. The orbital symmetry calculation of the thianthrene molecule using natural bond orbital (NBO)[57] analysis suggests that one of the lone pairs of sulfur is hybridized with s (65.38%) and p (34.61%), while the other retains its pure p character (Figure 3E). This characteristic of the thianthrene molecule is similar to that of thiophene featuring strongly delocalized p-orbitals. Notably, the thianthrene core also exhibits the overlap of one of the sulfur's nonbonding electrons with the 2p orbital of the neighboring carbon atom but to a weak extent (Figures 3E and S18). This "sp" mixing generates a 16π electron-rich thianthrene node with a weak aromatic character even though the carbon–sulfur bridge is out of the plane. Therefore, the 2D thianthrene-based COF is a unique example of a nonplanar weak aromatic system.

Sulfurization of the Thianthrene Structure. The redox affinity of the sulfur center and the high electron density on the framework structure render DUT-177 as an ideal candidate for charge storage. However, a typical lithium-ion battery half-cell which is fabricated from DUT-177 and a lithium metal reference electrode show irreversible COF degradation at 1.75 V, likely attributed to the carbon–sulfur bond cleavage and irreversible lithium salt deposition on the electrode (Figure S19). On the other hand, the dithiine linkage belongs to the category of the organo-polysulfanes with one sulfur atom covalently shared between two carbon atoms. In such systems, sulfur–sulfur affinity can be vital for the interconversion of organo-sulfur compounds into a higher number of sulfur-atom-containing analogues during sulfurization reactions. Thus, DUT-177 shows potential for postsynthetic modification via sulfurization. Here, the well-defined structure of the crystalline COF and its analogous model compound create a platform to obtain deep insights into the possible structural transformation. To investigate the possibility of the conversion of the dithiine linkage, the model compound was treated with excess sulfur at 180 °C under vacuum. Among the many possibilities, the conversion takes place on the sulfur bridge itself to generate a dithianthrene structure which is detectable via matrix-assisted laser desorption/ionization time of flight mass spectrometry (MALDI-TOF-MS) (Figures S20–S22). Additionally, the sulfurized model compound (S-model compound) was

https://doi.org/10.1021/jacs.2c02346
J. Am. Chem. Soc. XXXX, XXX, XXX–XXX

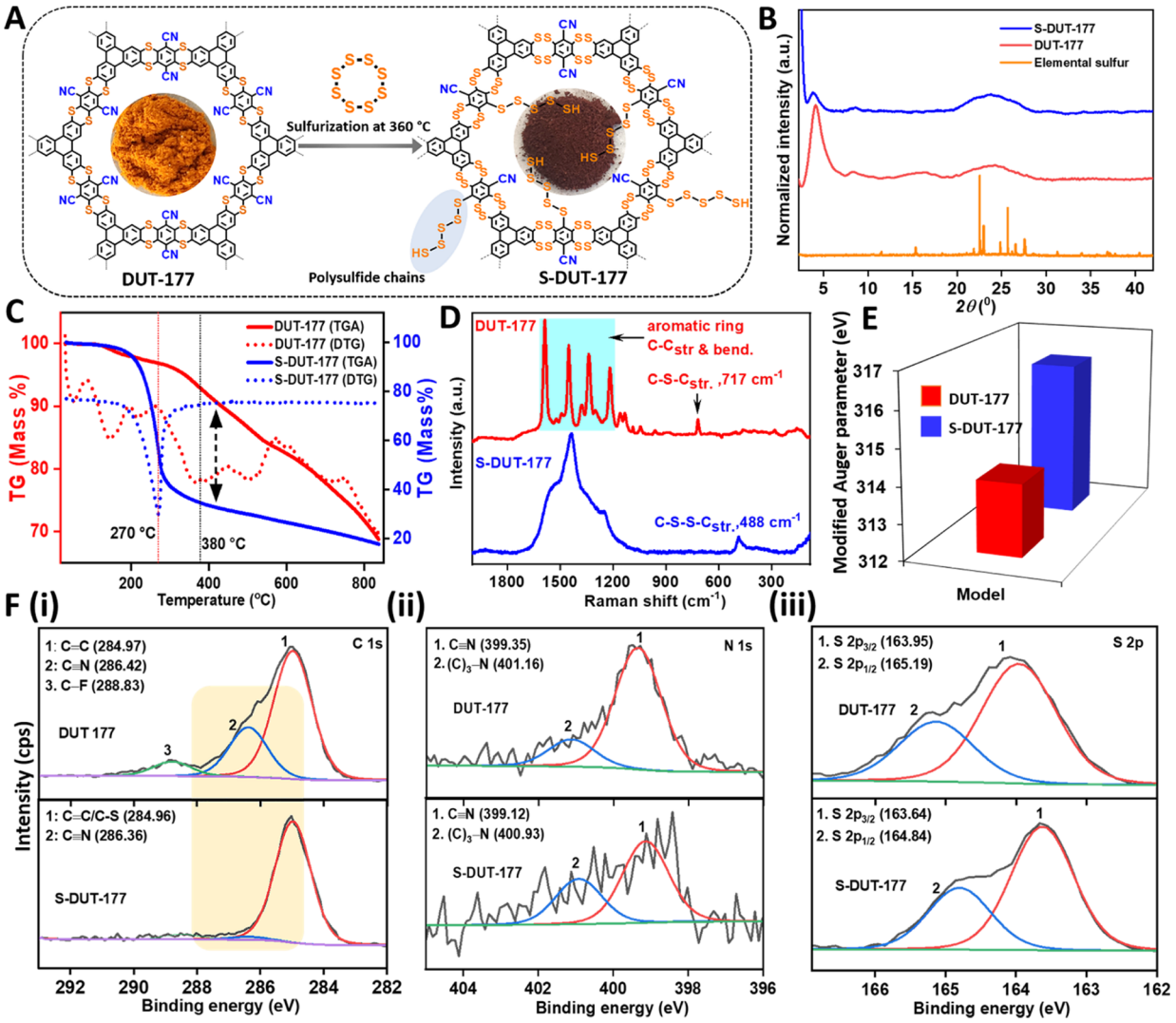

Figure 4. (A) Schematic illustration of the sulfurization of DUT-177 resulting in the formation of S-DUT-177 with covalently linked sulfur. (B) PXRD patterns of the as-made DUT-177, S-DUT-177, and elemental sulfur. (C) TGA-DTA plot of the as-made DUT-177 and S-DUT-177. (D) Raman shifts of the as-made DUT-177 with S-DUT-177. (E) Change of the modified Auger parameters from the S LMM Auger region of DUT-177 and S-DUT-177 estimated from Auger electron spectroscopy. (F) X-ray photoelectron spectroscopy analysis data of (i) C 1s, (ii) N 1s, and (iii) S 2p nuclei of DUT-177 and S-DUT-177. The yellow shaded area shows the marked decrease in nitrile's signal.

thoroughly characterized by CP-MAS-^{13}C NMR, Raman, and IR spectroscopies (Figure S23). These studies indicate the possible conversion of thianthrene to dithianthrene after sulfurization which is the first observation of this kind of transformation to the best of our knowledge.

A similar conversion was expected during the sulfurization of DUT-177; however, only molten sulfur pore adsorption was detected after sulfurization under similar reaction conditions. To optimize the covalent anchoring of sulfur, DUT-177 was soaked in a solution of sulfur in toluene, followed by evaporation of toluene. Afterward, the powder mixture was subjected to sulfurization under a vacuum of 10^{-4} (kPa) in a flame-sealed quartz ampoule by stepwise temperature increase (120 °C—2 h, 150 °C—6 h, 360 °C—12 h). Subsequently, excess elemental sulfur was removed using toluene to obtain a sulfurized version of DUT-177, named S-DUT-177, with most of the sulfur covalently anchored to the COF backbone (Figure 4A and Scheme S3). The obtained material lost its crystallinity, but no crystalline elemental sulfur impurity was observed by PXRD analysis (Figure 4B). The experimental data of S-DUT-177 strongly suggest the possible replacement of the nitrile substituents by polysulfide chains via a S_NAr pathway along with conversion to the dithianthrene linkage after sulfurization. The mechanism might be similar to the one reported by Thompson and Huestis.[58] We expect that polysulfides are likely to form highly basic radical dianions ($S_n^{2\bullet-}$) at a high temperature (360 °C),[59] which possibly substitute some of the nitrile groups to covalently anchor the polysulfide chains in a similar way. This enhances the percentage of the covalently integrated sulfur in the S-DUT-177 framework from 38 to 85% (calculated from the elemental analysis) which is even higher than that of the theoretically calculated sulfur content in the converted dithianthrene COF (Figures S24, S25 and Table S6). Anchoring of polysulfide chains has been previously reported and showed advantages for the use of the COFs in energy storage devices.[60] The scanning electron microscopy (SEM)−energy-dispersive X-ray (EDX) analysis mapping of S-DUT-177 supports a homogeneous distribution of sulfur throughout S-DUT-177 and confirms high sulfur loading throughout the carbon skeleton of the

https://doi.org/10.1021/jacs.2c02346
J. Am. Chem. Soc. XXXX, XXX, XXX−XXX

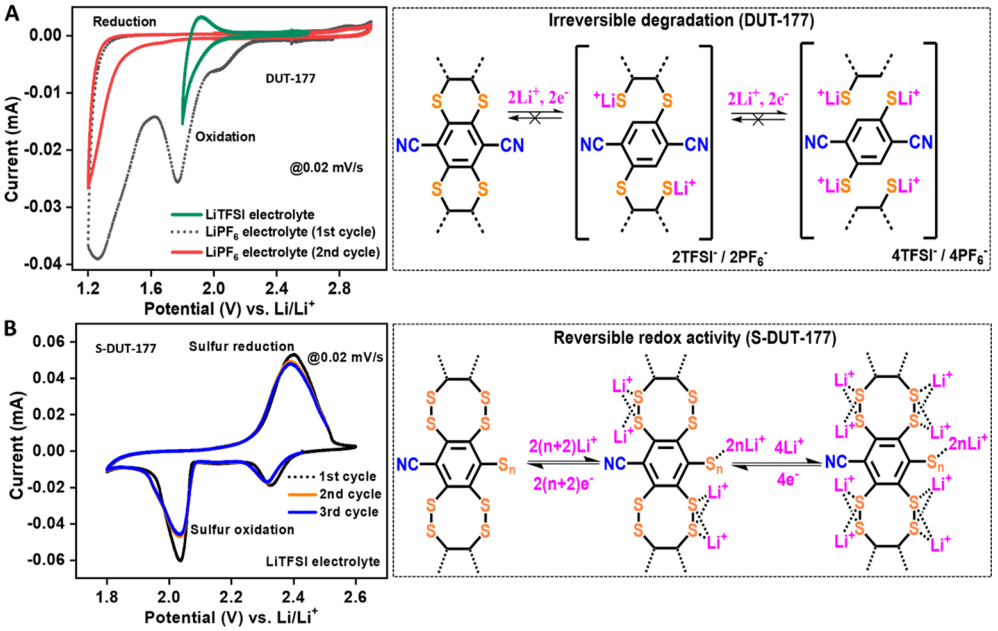

Figure 5. (A) CV measurement of a DUT-177-derived coin cell shows irreversible degradation of DUT-177 in different electrolyte systems. (Right) Depiction of a plausible degradation pathway upon the lithium interaction with the dithiine linkage of DUT-177. (B) CV measurement of the S-DUT-177-derived coin cell shows reversible oxidation−reduction. (Right) Illustration of a plausible reversible interaction mechanism of lithium ions with covalently anchored sulfur in S-DUT-177.

framework. Thermogravimetric analysis (TGA) coupled with mass spectrometry (MS) in synthetic air shows an early onset of the decomposition of S-DUT-177. The sulfur monoxide and sulfur dioxide releases from the sample are detected at 270 °C with nearly 62% weight loss, while the pristine DUT-177 degrades at 380 °C (Figures 4C and S26). This mass loss is attributed to covalently bound polysulfides attached to the pore wall of S-DUT-177. A drastic drop in porosity was observed after the sulfurization of DUT-177, although the chemical integrity remained, as confirmed from the characteristic IR stretching bands (Figure S26). The covalent anchoring of polysulfide by a partial replacement of the nitrile groups was confirmed by X-ray photoelectron spectroscopy (XPS) and IR spectroscopy, while the conversion from thianthrene to dithianthrene structures was detected by Auger electron spectroscopy (AES) and Raman studies of pristine DUT-177 and S-DUT-177 (Figures 4D−F). Though the profound sulfur electron density results in a substantial line broadening of the Raman shift of S-DUT-177, the drift of the stronger C−S−C linkage (788 cm^{-1}) to a weaker C−S−S−C linkage (418 cm^{-1}) is distinguishable. Substantial decrease of the N_{1s} signal in the XPS measurement of the COF after sulfurization and the disappearance of the C−N signal in the C_{1S} region suggest the covalent anchoring of polysulfide by partial substitution of the pseudo-halogen-type nitrile group (Figure 4Fi,ii). This is accompanied by shifting of the binding energy of S $2p_{1/2}$ and S $2p_{3/2}$ to a lower energy after the conversion to the easily ionizable dithianthrene unit (Figure 4F). The sulfurization of the model compound was performed at lower temperatures (180 °C) since the compound degraded at higher temperatures. Hence, a change in the binding energy was only observed for the S $2p_{1/2}$ and S $2p_{3/2}$ signals for thianthrene to dithianthrene conversion, while the C 1s and N 1s signals did not show any significant change (Figure S27). Therefore, the substitution of the thenitrile group with the polysulfide chain did not occur on the model compound. IR spectra of S-DUT-177 show a marked decrease of the strong signal of the −C═N stretching (2227 cm^{-1}) frequency. This also suggests partial substitution of nitrile groups. Furthermore, the appearance of terminal thiol (−SH) stretching frequencies (2662 cm^{-1}) clearly indicates the termination of the anchored polysulfide chains in S-DUT-177 which was not present in DUT-177 (Figure S26D).

However, due to similarities in electronegativity, the conversion of C−S−C bonds (thianthrene) to C−S−S−C bonds (dithianthrene) is hard to determine through the analysis of the traditional photoemission core electrons (C 1s and S 2p). One way in which changes to the sulfur bonding may be probed is through the measurement of the S LMM Auger region and subsequent calculation of the corresponding modified Auger parameter (*a'*) (Figure 4E). Analysis of *a'* may provide insights into the relaxation energy and screening of core holes located on the sulfur atom of interest.[61] If a system reports higher energy of *a'*, this indicates higher relaxation energy or improved screening of the core hole following photoemission. The dithiine-linked framework exhibits a higher Auger parameter following sulfurization (S-DUT-177) which indicates the formation of the dithianthrene ("C−S−S−C") linkage due to a higher number of valence electrons capable of screening the partner core hole via charge transfer (Figure S28 and Table S7). Importantly, this dithianthrene-linked S-DUT-177 is highly sensitive and degrades easily even in the presence of ambient atmosphere (Figure S29).

Activity of Covalently Anchored Polysulfide in Lithium−Sulfur Batteries. The presence of thianthrene and nitrile in these sulfur-linked COFs (thianthrene and dithianthrene structures) suggests cathodic activity against a lithium metal electrode in the higher potential window (1.2 to 2.8 V). The cyclic voltammogram of a coin cell derived from DUT-177 and a lithium metal reference electrode shows prominent and strong oxidation at 1.75 V at all analyzed scan rates while using lithium bis-(trifluoromethanesulfonyl)imide

https://doi.org/10.1021/jacs.2c02346
J. Am. Chem. Soc. XXXX, XXX, XXX−XXX

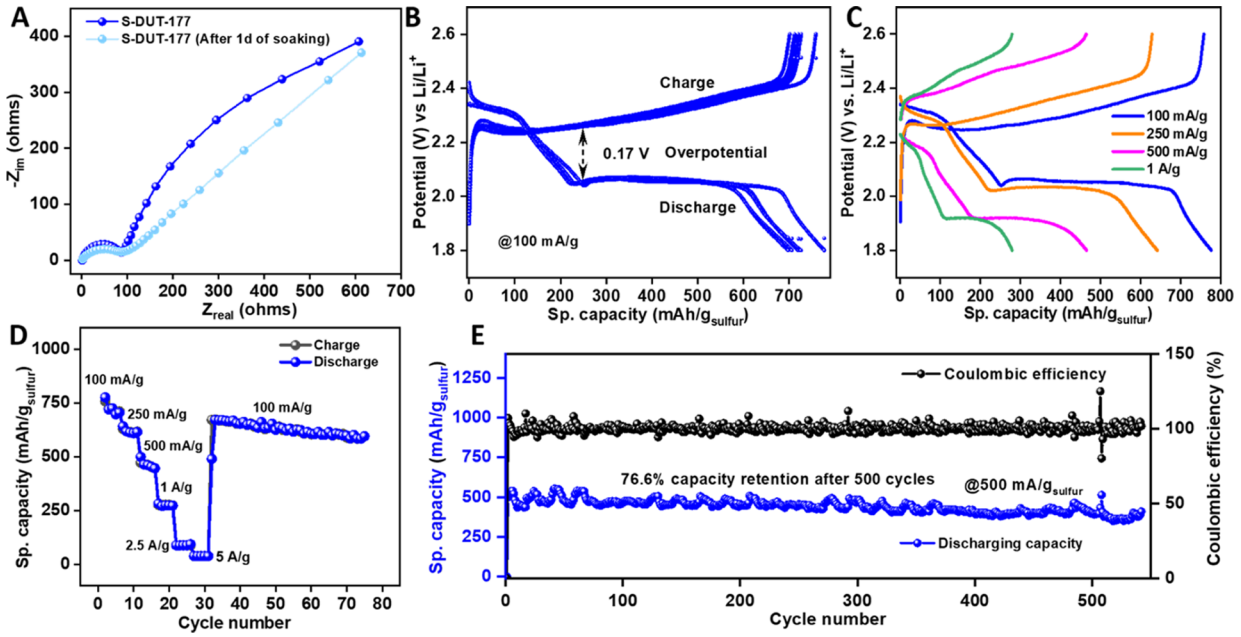

Figure 6. (A) Nyquist plots obtained from impedance measurements of the S-DUT-177-derived coin cell immediately after configuration of the coin cell (dark blue) and after 1 day of electrolyte wetting (light blue). (B,C) Charge−discharge profiles of the S-DUT-177-derived coin cell at different current densities. (D) Rate performance of the S-DUT-177-derived coin cell at different current densities. (E) Cycle stability of the S-DUT-177-derived coin cell at 500 mA/g current densities.

(LiTFSI) in dioxolane (DOL)/dimethoxyethane (DME) (1:1) with 0.1 M lithium nitrate ($LiNO_3$) as an electrolyte (Figure 5A). This oxidation also reduces the Coulombic efficiency of the battery since the oxidation capacity of the COF always remains higher than the reduction capacity. This eventually results in a drop in capacity with cycling. However, the reason behind the fading capacity was unexplored because this oxidation of the COF did not reach completion in each cycle in the restricted potential window of LiTFSI.[62] As an alternative, lithium hexafluorophosphate ($LiPF_6$) in an ethylene carbonate (EC)/dimethyl carbonate (DMC) (1:1) electrolyte with an enlarged potential window (1.2 to 2.8 V) was employed, and complete irreversible oxidation of DUT-177 was detected at 1.75 V and at 1.25 V in the very first cycle which is not observed in the subsequent cycles (Figure S30). This signifies irreversible degradation of DUT-177 probably due to the cleavage of the carbon−sulfur bond accompanied with the decomposition of the carbonate electrolyte by polysulfide species (Figure 5A). The strong affinity of sulfur to the lithium ion aids this degradation process which does not revert to the thianthrene unit during the following reduction cycle of DUT-177. Meanwhile, the dithianthrene structure and anchored polysulfide of S-DUT-177 interact with the lithium ions reversibly with the available lone pair electrons from the disulfide bridge ("S−S" linkage) (Figure 5B). The partial replacement of the nitrile group with covalently attached polysulfide entities starts reacting with the lithium ions from LiTFSI and shows reversible oxidation−reduction peaks in the cyclic voltammograms in the desired potential window (1.8 to 2.8 V) of the Li−S battery (Figure S31). The interaction of lithium ions with multiple sulfur atoms confirms the potential of exploiting this sulfurized COF (S-DUT-177) for an advanced Li−S battery. The Nyquist plot of the impedance analysis confirms a low resistivity (90 Ω) for the S-DUT-177-derived coin cell against high AC frequency but poor diffusivity of the lithium in the extremely low-frequency region (0.1 MHz) (Figure 6A). However, the impedance measured after 24 h of soaking the electrolyte shows drastic reduction of the diffusion resistance because of improved wettability of the electrode with the electrolyte. The improvement in the conductivity of the S-DUT-177-derived cathode was adjusted by a homogeneous mixing with 20% of super-P-carbon (Table S8). This makes S-DUT-177 a suitable cathode for facile lithium interactions and hence for effective lithium ion storage. The redox activity of the anchored polysulfide chains mostly contributes to the charge−discharge profile with a long-range voltage plateau at 2.08 V (Figure 6B), which delivers almost 72% of the total capacity with 99% Coulombic efficiency in each cycle. The minor contribution of the capacity at the voltage plateau of 2.35 V comes from unavoidable dissolution of the anchored polysulfide chain in the DOL/DME (1:1) medium which is unlike that of the sulfurized polyacrylonitrile (S-PAN).[63] However, this degradation process is slow and does not show any immediate impact on the overall battery performance. We must consider that one side of the polysulfide chain is directly attached to the framework's skeleton of S-DUT-177, while the other side remains free, leading to an irreversible reaction during the interaction with lithium. Though the nitrile substitutions are present in both DUT-177 and polyacrylonitrile, the chemical transformation products are not similar after sulfurization. The proposed in-plane ring-closure mechanism of nitrile groups in S-PAN is unlikely to happen in the stacked layers of the COF since the nitrile groups are present in subsequent layers. In this case, we expect the S_NAr reaction[58] for the partial replacement of the nitrile groups by polysulfides at elevated temperature since their diradical anion forms are highly basic and prone to react to form "S−C" bonds, while the other side of the sulfur chains remains unbound.[59]

This is in contrast to the S-PAN-derived cathode material where both ends of the polysulfide chains are covalently attached to the carbon backbone. Our investigation shows

https://doi.org/10.1021/jacs.2c02346
J. Am. Chem. Soc. XXXX, XXX, XXX−XXX

similarities to the work of Zhang and co-workers.[64] They described anchoring of polysulfide chains by substitution of fluorine atoms in a 2D COF (COF−F−S). However, this covalent sulfur attachment could not completely inhibit polysulfide dissolution. The TGA−differential thermal analysis (DTA) of the cycled (after 500 cycles) electrode shows a reduction of sulfur content by 14% (Figure S32).

Although the specific capacity (720 mA h/g@100 mA/g) achieved for S-DUT-177 is not higher compared with that of carbon-based cathodes, the results demonstrate that sulfur is electrochemically addressed at a lower overpotential (0.17 V) than that in the typical sulfur-impregnated electrodes.[65,66] The covalently anchored polysulfide and the lithium chelating effect of the disulfide ("S−S") moiety in the dithianthrene unit play a vital role in the reduction of the overpotential for charge−discharge. The lower gravimetric specific capacity (720 mA h/g@100 mA/g) in comparison to the theoretical value (1675 mA h/g) is attributed to poor electronic conductivity of the sulfurized COF (S-DUT-177). This hampers the electronic activation process of the anchored polysulfide during lithiation. As a result, the achieved specific capacity originating from the voltage plateau at 2.08 V gradually decreases with the increase of current density (at 1 A/g, the specific capacity is 276 mA h/g) (Figure 6C,D). It is interesting to see the improved rate performance of the polysulfur-anchored S-DUT-177 in comparison to most of the sulfur-impregnated porous COFs (Table S9).[64,67−72] Since the sulfur loading was possible only up to 0.55 mg/cm^2 in the S-DUT-177-derived electrode owing to the very low density of the material, the areal capacity (1.8 mA h/cm^2@0.25 mA/cm^2) is comparatively low. Also, in our derived electrode, the organic backbone contributes considerably to the weight along with the sulfur content. To enhance the sulfur-to-carbon backbone ratio in the polysulfide-anchored COF, we envision frameworks with smaller organic moieties but highly functionalized with substitutable functional groups for polysulfide anchoring. In this regard, formation of the anchored polysulfides with longer chains would be a better option.

The S-DUT-177-derived electrode soaks the electrolyte easily and initiates quick drying of the cell. Hence, the electrolyte-to-sulfur ratio (E/S) was kept higher (16 μL/mg$_S$) than the limits achieved for optimized pouch cells (3 to 10 μL/mg). This higher E/S maintains the reversibility of the redox reaction and retains the Coulombic efficiency and delivers 76.6% of the initial capacity even after 500 cycles while running the coin cell at 500 mA/g (Figure 6E), which is substantially better than the "COF−F−S" (64.5% retention after 100 cycles).[64] Hence, some inhibition of the shuttle effect (polysulfide dissolution in the Li−S battery) in the initial cycles was possible by covalently anchored sulfur entities in S-DUT-177.

CONCLUSIONS

The ring-closure mechanism during DUT-177 formation leads to a dithiine-linked framework featuring a weak aromatic ring current and a wavy-type stacking interaction between the layers of this COF and integrates fascinating electronic properties. This not only brings novel linkage chemistry to expand the family of 2D layered COFs but also offers a dynamic platform for postsynthetic modification. The sulfurization of the thianthrene COF shows the possibility of the interconversion to the dithianthrene structure as well as functionalization of the pore wall with the covalently anchored polysulfide chains by partial substitution of the nitrile moieties. This allows the sulfur entities to be redox-active owing to stable and reversible lithium interactions with the sulfurized framework. However, the sulfurization decreases the crystallinity of the framework, impeding mechanistic investigations of plausible Li framework−sulfur interactions. Improvement of design strategies and development of suitable linkers can enhance the inherent sulfur quantity in the framework to fulfill the requirements for improved cathodic activity in Li−S batteries. Strongly binding the sulfur to the framework via polysulfide rings or using polysulfide itself as the linkage for framework construction can potentially reduce the shuttle effect in higher electrochemical potential windows. Advanced COFs containing sulfur linkages may play an important role in improving the understanding of Li−S-batteries on a molecular level. In particular, electronically conductive frameworks will lead to a significantly improved overall battery performance.

ASSOCIATED CONTENT

Supporting Information

The Supporting Information is available free of charge at https://pubs.acs.org/doi/10.1021/jacs.2c02346.

Experimental procedures, NMR spectra, UV−vis, Raman studies, FTIR spectra, elemental analyses, PXRD patterns, nitrogen isotherms, BET plots, TGA data, FE-SEM images, HR-TEM images, XPS results, MALDI-TOF, and electrochemical methods and data (PDF)

Accession Codes

CCDC 2149889 contains the supplementary crystallographic data for this paper. These data can be obtained free of charge via www.ccdc.cam.ac.uk/data_request/cif, or by emailing data_request@ccdc.cam.ac.uk, or by contacting The Cambridge Crystallographic Data Centre, 12 Union Road, Cambridge CB2 1EZ, UK; fax: +44 1223 336033.

AUTHOR INFORMATION

Corresponding Authors

Sattwick Haldar − *Chair of Inorganic Chemistry I, Technische Universität Dresden, Dresden 01069, Germany;* orcid.org/0000-0001-9337-4287; Phone: 035146341127; Email: sattwick.haldar@tu-dresden.de

Stefan Kaskel − *Chair of Inorganic Chemistry I, Technische Universität Dresden, Dresden 01069, Germany; Fraunhofer Institute for Material and Beam Technology (IWS), Dresden 01277, Germany;* orcid.org/0000-0003-4572-0303; Email: stefan.kaskel@tu-dresden.de

Authors

Mingchao Wang − *Center for Advancing Electronics Dresden (cfaed) and Faculty of Chemistry and Food Chemistry, Technische Universität Dresden, Dresden 01069, Germany*

Preeti Bhauriyal − *Chair of Theoretical Chemistry, Technische Universität Dresden, Dresden 01069, Germany*

Arpan Hazra − *Chair of Inorganic Chemistry I, Technische Universität Dresden, Dresden 01069, Germany;* orcid.org/0000-0001-7383-7416

Arafat H. Khan − *Chair of Bioanalytical Chemistry, Technische Universität Dresden, Dresden 01069, Germany*

https://doi.org/10.1021/jacs.2c02346
J. Am. Chem. Soc. XXXX, XXX, XXX−XXX

Volodymyr Bon − *Chair of Inorganic Chemistry I, Technische Universität Dresden, Dresden 01069, Germany;* orcid.org/0000-0002-9851-5031
Mark A. Isaacs − *Department of Chemistry, University College London, London WC1H 0AJ, U.K.; HarwellXPS, Rutherford Appleton Laboratories, Research Complex at Harwell, Didcot OX11 0FA, U.K.;* orcid.org/0000-0002-0335-4272
Ankita De − *Chair of Inorganic Chemistry I, Technische Universität Dresden, Dresden 01069, Germany*
Leonid Shupletsov − *Chair of Inorganic Chemistry I, Technische Universität Dresden, Dresden 01069, Germany*
Tom Boenke − *Chair of Inorganic Chemistry I, Technische Universität Dresden, Dresden 01069, Germany; Fraunhofer Institute for Material and Beam Technology (IWS), Dresden 01277, Germany*
Julia Grothe − *Chair of Inorganic Chemistry I, Technische Universität Dresden, Dresden 01069, Germany*
Thomas Heine − *Chair of Theoretical Chemistry, Technische Universität Dresden, Dresden 01069, Germany;* orcid.org/0000-0003-2379-6251
Eike Brunner − *Chair of Bioanalytical Chemistry, Technische Universität Dresden, Dresden 01069, Germany;* orcid.org/0000-0003-3511-9899
Xinliang Feng − *Center for Advancing Electronics Dresden (cfaed) and Faculty of Chemistry and Food Chemistry, Technische Universität Dresden, Dresden 01069, Germany; Center for Advancing Electronics Dresden (cfaed) and Faculty of Chemistry and Food Chemistry, Technische Universität Dresden, Dresden 01062, Germany; Max Planck Institute of Microstructure Physics, Halle (Saale) 06120, Germany*
Renhao Dong − *Center for Advancing Electronics Dresden (cfaed) and Faculty of Chemistry and Food Chemistry, Technische Universität Dresden, Dresden 01069, Germany; Key Laboratory of Colloid and Interface Chemistry of the Ministry of Education, School of Chemistry and Chemical Engineering, Shandong University, Jinan 250100, China;* orcid.org/0000-0002-4125-9284
Andreas Schneemann − *Chair of Inorganic Chemistry I, Technische Universität Dresden, Dresden 01069, Germany;* orcid.org/0000-0001-6801-2735

Complete contact information is available at: https://pubs.acs.org/10.1021/jacs.2c02346

Notes

The authors declare no competing financial interest.

■ ACKNOWLEDGMENTS

This work was supported by the DFG Priority Programme "Polymer-based Batteries" (SPP 2248). The authors are grateful for the support from collaborative research center "Chemistry of Synthetic 2D Materials" funded by the Deutsche Forschungsgemeinschaft (DFG, German Research Foundation)—SFB-1415-417590517. P.B. acknowledges the Alexander von Humboldt Foundation for funding. A.S. gratefully acknowledges the Fonds der Chemischen Industrie for a Liebig Fellowship. The X-ray photoelectron (XPS) data collection was performed at the EPSRC National Facility for XPS ("HarwellXPS"), operated by Cardiff University and UCL, under contract no. PR16195. Single-crystal X-ray diffraction data have been collected on BL14.2 at the BESSY II electron storage ring operated by the Helmholtz-Zentrum Berlin. We would particularly like to acknowledge the help and support of Dr. U. Mueller and Dr. Th. Hauß during the experiment. We thank the Center for Information Services and High-Performance Computing (ZIH) at TU Dresden for generous allocations of computer time. We also acknowledge the use of the facilities in the Dresden Center for Nanoanalysis (DCN) at the Technische Universität Dresden.

■ REFERENCES

(1) Ding, S.-Y.; Wang, W. Covalent organic frameworks (COFs): from design to applications. *Chem. Soc. Rev.* **2013**, *42*, 548−568.
(2) Jin, Y.; Hu, Y.; Ortiz, M.; Huang, S.; Ge, Y.; Zhang, W. Confined growth of ordered organic frameworks at an interface. *Chem. Soc. Rev.* **2020**, *49*, 4637−4666.
(3) Diercks, C. S.; Yaghi, O. M. The atom, the molecule, and the covalent organic framework. *Science* **2017**, *355*, No. eaal1585.
(4) Geng, K.; He, T.; Liu, R.; Dalapati, S.; Tan, K. T.; Li, Z.; Tao, S.; Gong, Y.; Jiang, Q.; Jiang, D. Covalent Organic Frameworks: Design, Synthesis, and Functions. *Chem. Rev.* **2020**, *120*, 8814−8933.
(5) Huang, N.; Wang, P.; Jiang, D. Covalent organic frameworks: a materials platform for structural and functional designs. *Nat. Rev. Mater.* **2016**, *1*, 16068.
(6) Kandambeth, S.; Dey, K.; Banerjee, R. Covalent Organic Frameworks: Chemistry beyond the Structure. *J. Am. Chem. Soc.* **2019**, *141*, 1807−1822.
(7) Lohse, M. S.; Bein, T. Covalent Organic Frameworks: Structures, Synthesis, and Applications. *Adv. Funct. Mater.* **2018**, *28*, 1705553.
(8) Côté, A. P.; Benin, A. I.; Ockwig, N. W.; O'Keeffe, M.; Matzger, A. J.; Yaghi, O. M. Porous, Crystalline, Covalent Organic Frameworks. *Science* **2005**, *310*, 1166−1170.
(9) Uribe-Romo, F. J.; Hunt, J. R.; Furukawa, H.; Klöck, C.; O'Keeffe, M.; Yaghi, O. M. A Crystalline Imine-Linked 3-D Porous Covalent Organic Framework. *J. Am. Chem. Soc.* **2009**, *131*, 4570−4571.
(10) Ding, S.-Y.; Gao, J.; Wang, Q.; Zhang, Y.; Song, W.-G.; Su, C.-Y.; Wang, W. Construction of Covalent Organic Framework for Catalysis: Pd/COF-LZU1 in Suzuki−Miyaura Coupling Reaction. *J. Am. Chem. Soc.* **2011**, *133*, 19816−19822.
(11) Jin, E.; Asada, M.; Xu, Q.; Dalapati, S.; Addicoat, M. A.; Brady, M. A.; Xu, H.; Nakamura, T.; Heine, T.; Chen, Q.; Jiang, D. Two-dimensional sp^2 carbon−conjugated covalent organic frameworks. *Science* **2017**, *357*, 673−676.
(12) Pastoetter, D. L.; Xu, S.; Borrelli, M.; Addicoat, M.; Biswal, B. P.; Paasch, S.; Dianat, A.; Thomas, H.; Berger, R.; Reineke, S.; Brunner, E.; Cuniberti, G.; Richter, M.; Feng, X. Synthesis of Vinylene-Linked Two-Dimensional Conjugated Polymers via the Horner−Wadsworth−Emmons Reaction. *Angew. Chem., Int. Ed.* **2020**, *59*, 23620−23625.
(13) Park, S.; Liao, Z.; Ibarlucea, B.; Qi, H.; Lin, H. H.; Becker, D.; Melidonie, J.; Zhang, T.; Sahabudeen, H.; Baraban, L.; Baek, C. K.; Zheng, Z.; Zschech, E.; Fery, A.; Heine, T.; Kaiser, U.; Cuniberti, G.; Dong, R.; Feng, X. Two-Dimensional Boronate Ester Covalent Organic Framework Thin Films with Large Single Crystalline Domains for a Neuromorphic Memory Device. *Angew. Chem., Int. Ed.* **2020**, *59*, 8218−8224.
(14) Lyu, H.; Diercks, C. S.; Zhu, C.; Yaghi, O. M. Porous Crystalline Olefin-Linked Covalent Organic Frameworks. *J. Am. Chem. Soc.* **2019**, *141*, 6848−6852.
(15) Haase, F.; Lotsch, B. V. Solving the COF trilemma: towards crystalline, stable and functional covalent organic frameworks. *Chem. Soc. Rev.* **2020**, *49*, 8469−8500.
(16) Lei, Z.; Lucas, F. W. S.; Canales Moya, E.; Huang, S.; Rong, Y.; Wesche, A.; Li, P.; Bodkin, L.; Jin, Y.; Holewinski, A.; Zhang, W. Highly stable dioxin-linked metallophthalocyanine covalent organic frameworks. *Chin. Chem. Lett.* **2021**, *32*, 3799.
(17) Lu, M.; Zhang, M.; Liu, C. G.; Liu, J.; Shang, L. J.; Wang, M.; Chang, J. N.; Li, S. L.; Lan, Y. Q. Stable Dioxin-Linked Metallophthalocyanine Covalent Organic Frameworks (COFs) as

Photo-Coupled Electrocatalysts for CO2 Reduction. *Angew. Chem., Int. Ed.* **2021**, *60*, 4864−4871.
(18) Zhang, B.; Wei, M.; Mao, H.; Pei, X.; Alshmimri, S. A.; Reimer, J. A.; Yaghi, O. M. Crystalline Dioxin-Linked Covalent Organic Frameworks from Irreversible Reactions. *J. Am. Chem. Soc.* **2018**, *140*, 12715−12719.
(19) Guo, J.; Xu, Y.; Jin, S.; Chen, L.; Kaji, T.; Honsho, Y.; Addicoat, M. A.; Kim, J.; Saeki, A.; Ihee, H.; Seki, S.; Irle, S.; Hiramoto, M.; Gao, J.; Jiang, D. Conjugated organic framework with three-dimensionally ordered stable structure and delocalized π clouds. *Nat. Commun.* **2013**, *4*, 2736.
(20) Huang, N.; Lee, K. H.; Yue, Y.; Xu, X.; Irle, S.; Jiang, Q.; Jiang, D. A Stable and Conductive Metallophthalocyanine Framework for Electrocatalytic Carbon Dioxide Reduction in Water. *Angew. Chem., Int. Ed.* **2020**, *59*, 16587−16593.
(21) Zhong, H.; Wang, M.; Ghorbani-Asl, M.; Zhang, J.; Ly, K. H.; Liao, Z.; Chen, G.; Wei, Y.; Biswal, B. P.; Zschech, E.; Weidinger, I. M.; Krasheninnikov, A. V.; Dong, R.; Feng, X. Boosting the Electrocatalytic Conversion of Nitrogen to Ammonia on Metal-Phthalocyanine-Based Two-Dimensional Conjugated Covalent Organic Frameworks. *J. Am. Chem. Soc.* **2021**, *143*, 19992−20000.
(22) Waller, P. J.; AlFaraj, Y. S.; Diercks, C. S.; Jarenwattananon, N. N.; Yaghi, O. M. Conversion of Imine to Oxazole and Thiazole Linkages in Covalent Organic Frameworks. *J. Am. Chem. Soc.* **2018**, *140*, 9099−9103.
(23) Haase, F.; Troschke, E.; Savasci, G.; Banerjee, T.; Duppel, V.; Dörfler, S.; Grundei, M. M. J.; Burow, A. M.; Ochsenfeld, C.; Kaskel, S.; Lotsch, B. V. Topochemical conversion of an imine- into a thiazole-linked covalent organic framework enabling real structure analysis. *Nat. Commun.* **2018**, *9*, 2600.
(24) Singh, V.; Kim, J.; Kang, B.; Moon, J.; Kim, S.; Kim, W. Y.; Byon, H. R. Thiazole-Linked Covalent Organic Framework Promoting Fast Two-Electron Transfer for Lithium-Organic Batteries. *Adv. Energy Mater.* **2021**, *11*, 2003735.
(25) Wang, P.-L.; Ding, S.-Y.; Zhang, Z.-C.; Wang, Z.-P.; Wang, W. Constructing Robust Covalent Organic Frameworks via Multi-component Reactions. *J. Am. Chem. Soc.* **2019**, *141*, 18004−18008.
(26) Wei, P.-F.; Qi, M.-Z.; Wang, Z.-P.; Ding, S.-Y.; Yu, W.; Liu, Q.; Wang, L.-K.; Wang, H.-Z.; An, W.-K.; Wang, W. Benzoxazole-Linked Ultrastable Covalent Organic Frameworks for Photocatalysis. *J. Am. Chem. Soc.* **2018**, *140*, 4623−4631.
(27) Wang, G.-B.; Li, S.; Yan, C.-X.; Zhu, F.-C.; Lin, Q.-Q.; Xie, K.-H.; Geng, Y.; Dong, Y.-B. Covalent organic frameworks: emerging high-performance platforms for efficient photocatalytic applications. *J. Mater. Chem. A* **2020**, *8*, 6957−6983.
(28) Zhao, X.; Pachfule, P.; Thomas, A. Covalent organic frameworks (COFs) for electrochemical applications. *Chem. Soc. Rev.* **2021**, *50*, 6871−6913.
(29) Wang, W.; Zhao, W.; Xu, H.; Liu, S.; Huang, W.; Zhao, Q. Fabrication of ultra-thin 2D covalent organic framework nanosheets and their application in functional electronic devices. *Coord. Chem. Rev.* **2021**, *429*, 213616.
(30) Hu, Y.; Wayment, L. J.; Haslam, C.; Yang, X.; Lee, S.-h.; Jin, Y.; Zhang, W. Covalent organic framework based lithium-ion battery: Fundamental, design and characterization. *EnergyChem* **2021**, *3*, 100048.
(31) Chu, J.; Wang, Y.; Zhong, F.; Feng, X.; Chen, W.; Ai, X.; Yang, H.; Cao, Y. Metal/covalent-organic frameworks for electrochemical energy storage applications. *EcoMat* **2021**, *3*, No. e12133.
(32) Haldar, S.; Kushwaha, R.; Maity, R.; Vaidhyanathan, R. Pyridine-Rich Covalent Organic Frameworks as High-Performance Solid-State Supercapacitors. *ACS Mater. Lett.* **2019**, *1*, 490−497.
(33) Haldar, S.; Kaleeswaran, D.; Rase, D.; Roy, K.; Ogale, S.; Vaidhyanathan, R. Tuning the electronic energy level of covalent organic frameworks for crafting high-rate Na-ion battery anode. *Nanoscale Horiz.* **2020**, *5*, 1264−1273.
(34) Robertson, C. M.; Leitch, A. A.; Cvrkalj, K.; Reed, R. W.; Myles, D. J. T.; Dube, P. A.; Oakley, R. T. Enhanced Conductivity and Magnetic Ordering in Isostructural Heavy Atom Radicals. *J. Am. Chem. Soc.* **2008**, *130*, 8414−8425.
(35) Cusin, L.; Peng, H.; Ciesielski, A.; Samorì, P. Chemical Conversion and Locking of the Imine Linkage: Enhancing the Functionality of Covalent Organic Frameworks. *Angew. Chem., Int. Ed.* **2021**, *60*, 14236−14250.
(36) Li, X.; Wang, H.; Chen, H.; Zheng, Q.; Zhang, Q.; Mao, H.; Liu, Y.; Cai, S.; Sun, B.; Dun, C.; Gordon, M. P.; Zheng, H.; Reimer, J. A.; Urban, J. J.; Ciston, J.; Tan, T.; Chan, E. M.; Zhang, J.; Liu, Y. Dynamic Covalent Synthesis of Crystalline Porous Graphitic Frameworks. *Chem* **2020**, *6*, 933−944.
(37) Segura, J. L.; Royuela, S.; Mar Ramos, M. Post-synthetic modification of covalent organic frameworks. *Chem. Soc. Rev.* **2019**, *48*, 3903−3945.
(38) Ding, H.; Mal, A.; Wang, C. Tailored covalent organic frameworks by post-synthetic modification. *Mater. Chem. Front.* **2020**, *4*, 113−127.
(39) Zhang, C.; Mahmood, N.; Yin, H.; Liu, F.; Hou, Y. Synthesis of Phosphorus-Doped Graphene and its Multifunctional Applications for Oxygen Reduction Reaction and Lithium Ion Batteries. *Adv. Mater.* **2013**, *25*, 4932−4937.
(40) Yang, Z.; Yao, Z.; Li, G.; Fang, G.; Nie, H.; Liu, Z.; Zhou, X.; Chen, X. a.; Huang, S. Sulfur-Doped Graphene as an Efficient Metal-free Cathode Catalyst for Oxygen Reduction. *ACS Nano* **2012**, *6*, 205−211.
(41) Ding, J.; Liu, Z.; Zhao, W.; Jin, W.; Xiang, L.; Wang, Z.; Zeng, Y.; Zou, Y.; Zhang, F.; Yi, Y.; Diao, Y.; McNeill, C. R.; Di, C. a.; Zhang, D.; Zhu, D. Selenium-Substituted Diketopyrrolopyrrole Polymer for High-Performance p-Type Organic Thermoelectric Materials. *Angew. Chem., Int. Ed.* **2019**, *58*, 18994−18999.
(42) Guan, X.; Li, H.; Ma, Y.; Xue, M.; Fang, Q.; Yan, Y.; Valtchev, V.; Qiu, S. Chemically stable polyarylether-based covalent organic frameworks. *Nat. Chem.* **2019**, *11*, 587−594.
(43) Ji, W.; Guo, Y.-S.; Xie, H.-M.; Wang, X.; Jiang, X.; Guo, D.-S. Rapid microwave synthesis of dioxin-linked covalent organic framework for efficient micro-extraction of perfluorinated alkyl substances from water. *J. Hazard. Mater.* **2020**, *397*, 122793.
(44) Ong, W. J.; Swager, T. M. Dynamic self-correcting nucleophilic aromatic substitution. *Nat. Chem.* **2018**, *10*, 1023−1030.
(45) Rangappa, P.; Shine, H. J. An overview of some reactions of thianthrene cation radical. Products and mechanisms of their formation. *J. Sulfur Chem.* **2006**, *27*, 617−664.
(46) Speer, M. E.; Kolek, M.; Jassoy, J. J.; Heine, J.; Winter, M.; Bieker, P. M.; Esser, B. Thianthrene-functionalized polynorbornenes as high-voltage materials for organic cathode-based dual-ion batteries. *Chem. Commun.* **2015**, *51*, 15261−15264.
(47) Dong, R.; Pfeffermann, M.; Liang, H.; Zheng, Z.; Zhu, X.; Zhang, J.; Feng, X. Large-Area, Free-Standing, Two-Dimensional Supramolecular Polymer Single-Layer Sheets for Highly Efficient Electrocatalytic Hydrogen Evolution. *Angew. Chem., Int. Ed.* **2015**, *54*, 12058−12063.
(48) Clough, A. J.; Yoo, J. W.; Mecklenburg, M. H.; Marinescu, S. C. Two-Dimensional Metal−Organic Surfaces for Efficient Hydrogen Evolution from Water. *J. Am. Chem. Soc.* **2015**, *137*, 118−121.
(49) Dong, R.; Han, P.; Arora, H.; Ballabio, M.; Karakus, M.; Zhang, Z.; Shekhar, C.; Adler, P.; Petkov, P. S.; Erbe, A.; Mannsfeld, S. C. B.; Felser, C.; Heine, T.; Bonn, M.; Feng, X.; Cánovas, E. High-mobility band-like charge transport in a semiconducting two-dimensional metal−organic framework. *Nat. Mater.* **2018**, *17*, 1027−1032.
(50) Pawley, G. S. Unit-cell refinement from powder diffraction scans. *J. Appl. Crystallogr.* **1981**, *14*, 357−361.
(51) M. J., Frisch; G. W., Trucks; H. B., Schlegel; G. E., Scuseria; M. A., Robb; J. R., Cheeseman; G., Scalmani; V., Barone; G. A., Petersson; H., Nakatsuji; X., Li; M., Caricato; A., Marenich; J., Bloino; B. G., Janesko; R., Gomperts; B., Mennucci; H. P., Hratchian; J. V., Ortiz; A. F., Izmaylov; J. L., Sonnenberg; D., Williams-Young; F., Ding; F., Lipparini; F., Egidi; J., Goings; B., Peng; A., Petrone; T., Henderson; D., Ranasinghe; V. G., Zakrzewski; J., Gao; N., Rega; G., Zheng; W., Liang; M., Hada; M., Ehara; K., Toyota; R., Fukuda; J.,

https://doi.org/10.1021/jacs.2c02346
J. Am. Chem. Soc. XXXX, XXX, XXX−XXX

Hasegawa; M., Ishida; T., Nakajima; Y., Honda; O., Kitao; H., Nakai; T., Vreven; K., Throssell; J. A., Montgomery, Jr.; J. E., Peralta; F., Ogliaro; M., Bearpark; J. J., Heyd; E., Brothers; K. N., Kudin; V. N., Staroverov; T., Keith; R., Kobayashi; J., Normand; K., Raghavachari; A., Rendell; J. C., Burant; S. S., Iyengar; J., Tomasi; M., Cossi; J. M., Millam; M., Klene; C., Adamo; R., Cammi; J. W., Ochterski; R. L., Martin; K., Morokuma; O., Farkas; J. B., Foresman; D. J., Fox *Gaussian 09*, Revision D. 01; Gaussian: Wallingford, CT, 2009.

(52) Perdew, J. P.; Burke, K.; Ernzerhof, M. Generalized Gradient Approximation Made Simple. *Phys. Rev. Lett.* **1996**, *77*, 3865−3868.

(53) Heyd, J.; Peralta, J. E.; Scuseria, G. E.; Martin, R. L. Energy band gaps and lattice parameters evaluated with the Heyd-Scuseria-Ernzerhof screened hybrid functional. *J. Chem. Phys.* **2005**, *123*, 174101.

(54) Khan, A. H.; Barth, B.; Hartmann, M.; Haase, J.; Bertmer, M. Nitric Oxide Adsorption in MIL-100(Al) MOF Studied by Solid-State NMR. *J. Phys. Chem. C* **2018**, *122*, 12723−12730.

(55) Kubo, A.; Spaniol, T. P.; Terao, T. The Effect of Bulk Magnetic Susceptibility on Solid State NMR Spectra of Paramagnetic Compounds. *J. Magn. Reson.* **1998**, *133*, 330−340.

(56) Alla, M.; Lippmaa, E. Resolution limits in magic-angle rotation NMR spectra of polycrystalline solids. *Chem. Phys. Lett.* **1982**, *87*, 30−33.

(57) Glendening, E. D.; Reed, A. E.; Carpenter, J. E.; Weinhold, F. *NBO*, version 3.1; Gaussian Inc.: Pittsburgh, 2003.

(58) Thompson, A. D.; Huestis, M. P. Cyanide Anion as a Leaving Group in Nucleophilic Aromatic Substitution: Synthesis of Quaternary Centers at Azine Heterocycles. *J. Org. Chem.* **2013**, *78*, 762−769.

(59) Steudel, R.; Chivers, T. The role of polysulfide dianions and radical anions in the chemical, physical and biological sciences, including sulfur-based batteries. *Chem. Soc. Rev.* **2019**, *48*, 3279−3319.

(60) Xu, F.; Yang, S.; Chen, X.; Liu, Q.; Li, H.; Wang, H.; Wei, B.; Jiang, D. Energy-storage covalent organic frameworks: improving performance via engineering polysulfide chains on walls. *Chem. Sci.* **2019**, *10*, 6001−6006.

(61) Thøgersen, A.; Diplas, S.; Mayandi, J.; Finstad, T.; Olsen, A.; Watts, J. F.; Mitome, M.; Bando, Y. An experimental study of charge distribution in crystalline and amorphous Si nanoclusters in thin silica films. *J. Appl. Phys.* **2008**, *103*, 24308.

(62) Li, G.; Li, Z.; Zhang, B.; Lin, Z. Developments of Electrolyte Systems for Lithium−Sulfur Batteries: A Review. *Front. Energy Res.* **2015**, *3*, 5.

(63) Mukkabla, R.; Buchmeiser, M. R. Cathode materials for lithium−sulfur batteries based on sulfur covalently bound to a polymeric backbone. *J. Mater. Chem. A* **2020**, *8*, 5379−5394.

(64) Wang, D.-G.; Li, N.; Hu, Y.; Wan, S.; Song, M.; Yu, G.; Jin, Y.; Wei, W.; Han, K.; Kuang, G.-C.; Zhang, W. Highly Fluoro-Substituted Covalent Organic Framework and Its Application in Lithium−Sulfur Batteries. *ACS Appl. Mater. Interfaces* **2018**, *10*, 42233−42240.

(65) Guo, J.; Xu, Y.; Wang, C. Sulfur-Impregnated Disordered Carbon Nanotubes Cathode for Lithium−Sulfur Batteries. *Nano Lett.* **2011**, *11*, 4288−4294.

(66) He, N.; Zhong, L.; Xiao, M.; Wang, S.; Han, D.; Meng, Y. Foldable and High Sulfur Loading 3D Carbon Electrode for High-performance Li-S Battery Application. *Sci. Rep.* **2016**, *6*, 33871.

(67) Lu, B.-Y.; Wang, Z.-Q.; Cui, F.-Z.; Li, J.-Y.; Han, X.-H.; Qi, Q.-Y.; Ma, D.-L.; Jiang, G.-F.; Zeng, X.-X.; Zhao, X. A Covalent Organic Framework with Extended π-Conjugated Building Units as a Highly Efficient Recipient for Lithium−Sulfur Batteries. *ACS Appl. Mater. Interfaces* **2020**, *12*, 34990−34998.

(68) Li, Z.; Zhou, H.-Y.; Zhao, F.-L.; Wang, T.-X.; Ding, X.; Han, B.-H.; Feng, W. Three-dimensional Covalent Organic Frameworks as Host Materials for Lithium-Sulfur Batteries. *Chin. J. Polym. Sci.* **2020**, *38*, 550−557.

(69) Duan, H.; Li, K.; Xie, M.; Chen, J.-M.; Zhou, H.-G.; Wu, X.; Ning, G.-H.; Cooper, A. I.; Li, D. Scalable Synthesis of Ultrathin Polyimide Covalent Organic Framework Nanosheets for High-Performance Lithium−Sulfur Batteries. *J. Am. Chem. Soc.* **2021**, *143*, 19446−19453.

(70) Zhu, Y.; Yang, J.; Qiu, X.; Li, M.; He, G.; Wang, Q.; Xie, Z.; Li, X.; Yu, H. Amphiphilic Carborane-Based Covalent Organic Frameworks as Efficient Polysulfide Nano-Trappers for Lithium−Sulfur Batteries. *ACS Appl. Mater. Interfaces* **2021**, *13*, 60373−60383.

(71) Ghazi, Z. A.; Zhu, L.; Wang, H.; Naeem, A.; Khattak, A. M.; Liang, B.; Khan, N. A.; Wei, Z.; Li, L.; Tang, Z. Efficient Polysulfide Chemisorption in Covalent Organic Frameworks for High-Performance Lithium-Sulfur Batteries. *Adv. Energy Mater.* **2016**, *6*, 1601250.

(72) Meng, Y.; Lin, G.; Ding, H.; Liao, H.; Wang, C. Impregnation of sulfur into a 2D pyrene-based covalent organic framework for high-rate lithium−sulfur batteries. *J. Mater. Chem. A* **2018**, *6*, 17186−17191.

https://doi.org/10.1021/jacs.2c02346
J. Am. Chem. Soc. XXXX, XXX, XXX−XXX